Inorganic Chemistry

Article

pubs.acs.org/IC

Manganese K-Edge X-Ray Absorption Spectroscopy as a Probe of the Metal–Ligand Interactions in Coordination Compounds

Michael Roemelt,[†] Martha A. Beckwith,[†,‡] Carole Duboc,[§] Marie-Noëlle Collomb,[§] Frank Neese,*[,†] and Serena DeBeer*[,†,‡]

[†]Max-Planck-Institut für Bioanorganische Chemie, Stiftstrasse 34-36, D-45470 Mülheim an der Ruhr, Germany

[‡]Department of Chemistry and Chemical Biology, Cornell University, Ithaca, New York 14853, United States

[§]Université Joseph Fourier Grenoble 1/CNRS, Département de Chimie Moléculaire, UMR-5250, Laboratoire de Chimie Inorganique Redox, Institut de Chimie Moléculaire de Grenoble FR- CNRS-2607, BP-53, 38041 Grenoble Cedex 9, France

Supporting Information

ABSTRACT: A series of manganese coordination compounds has been investigated by X-ray absorption spectroscopy (XAS). The K-pre-edge spectra are interpreted with the aid of time-dependent density functional theory (TD-DFT). This method was calibrated for the prediction of manganese K-pre-edges with different functionals. Moreover the nature of all observed features could be identified and classified according to the corresponding set of acceptor orbitals, either 1s to 3d transitions or metal-to-ligand charge transfer (MLCT) bands. The observable MLCT bands are further divided into features that correspond to transitions into empty π^* orbitals of π-donor ligands and those of π-acceptor ligands. The ability to computationally reproduce the observed features at the correct relative transition energy is strongly dependent on the nature of the transition. A detailed analysis of the electronic structure of a series of Mn coordination compounds reveals that the different classes of observable transitions provide added insight into metal–ligand bonding interactions.

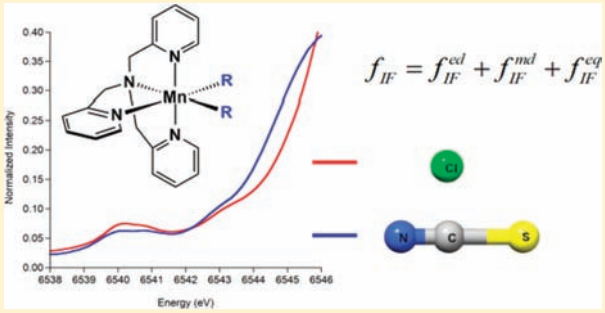

INTRODUCTION

Transition metal K-edge absorption spectroscopy is a powerful tool for the investigation of the electronic and geometric structure of inorganic and bioinorganic coordination compounds.[1−4] It is a highly element-specific technique and therefore has been applied extensively to large systems containing transition metals, such as the active sites of enzymes. In conjunction with other spectroscopic techniques, it provides a means to experimentally assess oxidation state, spin state, and symmetry of the respective transition metal absorber.[5−9] Transition metal K-edge spectra can be divided into two parts, each containing valuable information about the system under consideration. The extended X-ray absorption fine structure (EXAFS) region at higher energies is used to determine metal to ligand bond distances and coordination numbers. The pre-edge and edge regions of the spectrum, which appear at lower energies, contain information about the electronic structure and geometric parameters such as site symmetry. In most cases, the shape and position of a transition metal K-edge are used as a "fingerprint" for electronic structure parameters, where assignments of oxidation state and spin state are based on empirical comparisons with known model complexes. Nevertheless, extensive efforts have been made using both molecular orbital and multiple scattering based approaches to obtain a more quantitative analysis of the edge region. In particular, a recent study by Jaszewski et al. showed that time-dependent density functional theory (TD-DFT) reproduces the experimentally observed correlation between the Mn oxidation state for Mn K-edge and L-edge rising edge energies.[10] In the current study, we focus on a detailed analysis of the pre-edge.

The weak pre-edge features of transition metal K-edge spectra have been analyzed using qualitative arguments such as site symmetry and ligand-field strength for quite some time.[1,2,11−14] Recently, we have developed a more quantitative approach for the prediction of pre-edge energies and intensities of iron, chlorine, and sulfur K-edges for model compounds using TD-DFT.[15−17] Within this approach one solves the time-dependent linear response equations of singly excited Kohn–Sham determinants where only the metal (or ligand) 1s orbital is allowed to donate an electron to the empty valence shell. The method yields transition energies and oscillator strengths for a preset number of excited states, which are all mutually orthogonal to each other. The description of the core hole leads to a systematic error in the absolute transition energies which can be compensated by a constant energy shift.[15] This energy shift is characteristic for each functional and basis set and hence has to be calibrated for different computational approaches.[16,17]

Received: October 14, 2011
Published: December 6, 2011

Table 1. Comparison of Experimental Pre-Edge Energies and Intensities to Calculated Values Using the B3LYP Functional

	experiment			calculation		
compound	energy [eV]	area[a]	reference[b]	energy [eV][c]	intensity	predicted experimental area[d]
$[Mn(III)(acac)_3]$	6540.2	4.5		6540.4	0.28	3.5
	6542.2	1.6		6541.9	0.14	2.6
$[Mn(III)(bpea)(N_3)_3]$	6540.5	4.8	21	6540.4	0.35	3.9
$[Mn(III)(phenylterpy)Cl_3]$	6540.3	3.8	22	6540.4	0.23	3.1
	6541.8	0.4		6541.6	0.10	2.4
[Mn(III)(salen)Cl]	6540.6	13.2		6541.2	2.04	14.0
	6542.6	0.6		6542.8	0.18	2.9
$[Mn(III)(terpy)Cl_3]$	6540.2	5.5	22	6540.4	0.24	3.2
$[Mn(III)(terpy)F_3]$	6540.7	4.2	21	6540.4	0.24	3.2
	6541.9	1.2		6541.9	0.31	3.7
$[Mn(III)(terpy)(N_3)_3]$	6540.2	4.1	23	6540.4	0.30	3.6
$[Mn(III)(tolylterpy)_2]^{3+}$	6540.1	6.0	24	6540.1	0.42	4.3
	6541.8	1.5		6542.0	0.13	2.6
$[Mn(II)(tbu_3terpy)_2]^{2+}$	6540.0	9.4	25	6540.1	0.95	7.5
$[Mn(II)(tbu_3terpy)(N_3)_2]$	6540.2	12.6	26	6540.2	1.92	13.3
$[Mn(II)(terpy)Cl_2]$	6540.2	11.0	27	6540.2	1.48	10.7
$[Mn(II)(terpy)(NO_3)_2(H_2O)]$	6540.3	5.9	28	6540.2	0.91	7.2
$[Mn(II)(CF_3CO_2)_2(terpy)(H_2O)]$	6540.2	8.1	29	6540.2	0.59	5.4
$[Mn(II)(tolylterpy)_2]^{2+}$	6540.0	8.4	24,30	6540.1	0.92	7.3
$[Mn(II)(tpa)Cl_2]$	6540.2	5.5	31	6540.3	0.51	4.8
$[Mn(II)(tpa)(NCS)_2]$	6540.0	4.0	25	6539.9	0.34	3.8
	6541.0	1.8		6540.8	0.55	5.1

[a]Experimental areas have been multiplied by 100. [b]Synthesis and crystallographic structure references. [c]The calculated energies have been shifted by 32.6 eV to higher energies. [d]The predicted experimental area, A, is obtained from the calculated intensity, I, according to $A = 6.01I + 1.79$. The calculated intensity is obtained as described in the Supporting Information.

In this work, we extend the existing method to mononuclear manganese coordination complexes (many of which were also examined previously using X-ray emission spectroscopy (XES)[18]) to make it available for the prediction of X-ray absorption spectroscopy (XAS) spectra of biologically relevant systems such as the oxygen evolving complex of photosystem II (PSII).[19,20] The method is calibrated for one meta-GGA functional (BP) and three hybrid functionals in conjunction with the triple-ζ basis set TZVP. Furthermore, we investigate the interaction of π-donor and acceptor ligands with the central manganese ion and examine their effect on the pre-edge and edge region of the XAS spectrum.

MATERIALS AND METHODS

A set of 16 mononuclear manganese complexes was selected as a calibration set. The molecular formulas, synthetic procedures, and structural references (when available) are given in Table 1. The following abbreviations have been used for the ligands: acac = acetyl acetonate; bpea = *N,N*-bis(2-pyridylmethyl)-ethylamine; salen = ethylenebis(salicylimine); tbu_3terpy = 4,4′,4″-tri-*tert*-butyl-2,2′:6′,2″-terpyridine; terpy = 2,2′:6′,2″-terpyridine; tolylterpy = 4′-(4-methylphenyl)-2,2′:6′,2″-terpyridine; phenylterpy = 4′-phenyl-2,2′:6′,2″-terpyridine; tpa = tris-2-picolylamine. A schematic representation of the structures is given in Scheme 1.

Sample Preparation. Samples were synthesized according to published procedures, as referenced in Table 1.[21−31] All XAS samples were prepared as dilutions in boron nitride, pressed in Al spacers, and sealed with 38 μm Kapton windows. All samples were measured at 10 K in a liquid Helium cryostat.

XAS Measurements. All XAS data were recorded at the Stanford Synchrotron Radiation Laboratory (SSRL) on focused beamline 9-3, under ring conditions of 3 GeV and 80−100 mA. A Si(220) monochromator was used for energy selection. A Rh-coated mirror (set to a cutoff of 10 keV) was used for harmonic rejection, in combination with 25% detuning of the monochromator. All data were measured in transmission mode. Internal energy calibration was performed by simultaneous measurement of the absorption of a Mn foil placed between a second and third ionization chamber. The first inflection point of the Mn foil was assigned to 6539.0 eV. Samples were monitored for photoreduction throughout the course of data collection. Only those scans which showed no evidence of photoreduction were used in the final averages. The averaged data were processed as described previously.[32]

Computational Details. All DFT calculations presented in this work were performed using the ORCA program package.[33] Scalar relativistic effects were taken into account at the ZORA level.[34,35] Open-shell species were treated with the spin-unrestricted Kohn−Sham method. All calculations used dense integration grids (ORCA Grid4).

Geometry Optimizations. All molecular geometries were optimized using the BP86 functional[36,37] together with scalar relativistically recontracted (SARC)[38] all electron def2-TZVP(-f) basis sets.[39] The Coulomb fitting basis of Weigend[40] was used in uncontracted form. Dichloromethane was chosen as the solvent within the conductor like screening model[41] (COSMO, $\varepsilon = 9.08$).

XAS Calculations. Manganese K-edge absorption spectra were investigated with a TD-DFT approach applying the Tamm−Dancoff approximation.[42] XAS calculations were performed with the BP,[36,37] B3LYP,[43,44] and the TPSSh[45] functionals. Additionally, a series of calculations with functionals of the hybrid form that use an exchange-correlation energy according to[46]

$$E_{XC} = aE_X^{HF} + (1-a)E_X^{LSD} + bE_X^{B88} + E_C^{LSD} + c(E_C^{LYP} - E_C^{LSD}) \quad (1)$$

was conducted. The exchange correlation energy appears as a weighted sum of the Hartree−Fock (HF) exchange (E_X^{HF}), the LSD exchange and correlation functional (E_X^{LSD}, E_C^{LSD}) of Vosko et al,[47] Becke's exchange functional (E_X^{B88})[36] and the correlation functional proposed by Lee, Yang, and Parr (E_C^{LYP}).[44] In the case of B3LYP the three parameters a, b, and c were chosen to be $a = 0.20$, $b = 0.72$, and

dx.doi.org/10.1021/ic202229b | Inorg. Chem. 2012, 51, 680−687

Scheme 1. Sixteen Manganese Model Complexes Investigated in This Study

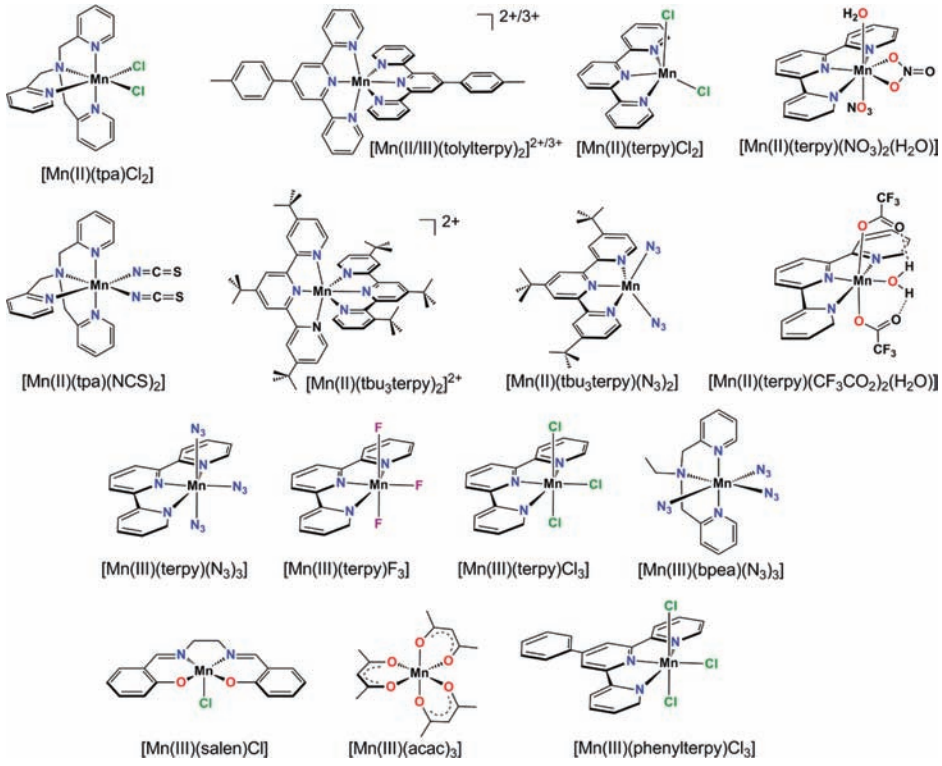

$c = 0.81$ on the basis of thermodynamic reference data. For the present purpose the amount of Hartree−Fock exchange, a, was varied between 0.0 and 0.3 (see below). When exact HF exchange was included, the RIJCOSX approximation[48] was employed within the SCF and the TD-DFT parts of the calculation. The conductor-like screening model was used to model a solution environment with acetonitrile ($\varepsilon = 36.6$) as the solvent. Absorption spectra were obtained from the TD-DFT calculations by applying a Gaussian fit with a broadening of 1 eV. In calculating the oscillator strength f_{IF} of a given transition between the states $|I\rangle$ and $|F\rangle$, electric dipole, magnetic dipole, and electric quadrupole contributions were included:[16,49]

$$
\begin{aligned}
f_{IF} &= f_{IF}^{ed} + f_{IF}^{md} + f_{IF}^{eq} \\
f_{IF}^{ed} &= \frac{2}{3} E_{FI} |\langle I|\hat{\mu}|F\rangle|^2 \\
f_{IF}^{md} &= \frac{2}{3}\alpha^2 E_{FI} |\langle I|\hat{M}|F\rangle|^2 \\
&= \frac{2}{3}\alpha^2 E_{FI} \left| \left\langle I \left| \sum_i \frac{1}{2}(\hat{l}(i) + 2\hat{s}(i)) \right| F \right\rangle \right|^2 \\
f_{IF}^{eq} &= \frac{1}{20}\alpha^2 E_{FI}^3 \sum_{a,b}^{x,y,z} |\langle I|\hat{Q}_{ab}|F\rangle|^2
\end{aligned}
\tag{2}
$$

Here, E_{FI} is the transition energy and α the fine structure constant, whereas $\hat{\boldsymbol{\mu}}$, $\hat{\mathbf{M}}$, and $\hat{\mathbf{Q}}$ denote the electric dipole, magnetic dipole and electric quadrupole moments operators.

RESULTS

Experimentally obtained Mn K-edge transition energies and intensities of the 16 model complexes and the corresponding calculated parameters using the B3LYP functional together with the computational model described above are summarized in Table 1. Tables containing the calculated parameters using the functionals BP86, TPSSh and a purpose specific functional described below, can be found in the Supporting Information. Figure 1a contains a comparison of the experimental transition energies and their calculated counterparts. In previous studies, we have established that a constant shift of the calculated energies accounts for most of the systematic error made by the TD-DFT method.[15−17] The exact size of the shift is dependent on the computational method and hence has to be calibrated for each combination of functional and basis set. A regression analysis of the data leads to an average energy shift of 32.6 eV (±0.2 eV). It should be noted that for the evaluation of this shift, only transitions with dominant 1s to 3d character (vide infra) were taken into account. Figure 1b shows the relationship between the experimental and calculated intensities of the pre-edge transitions. The linear relationship shows a correlation constant of $R = 0.90$. This is somewhat inferior to the correlation obtained for the transition energies but is still considered satisfactory (Table 1).

Symmetry and Ligand Field Effects on the 1s→3d Transitions. In our previous study of the K-pre-edges of several Fe-compounds, the relationship between the shape and intensity of the pre-edges and the geometric and electronic structure of the complexes was examined.[15] Similar arguments hold for the present series of Mn complexes. Figure 2 shows the comparison of the measured (a) and calculated (b) pre-edges of representative members of the calibration series. A complete comparison for all compounds may be found in the Supporting Information, Figure S1−S6. On the basis of these spectra, some general trends may be noted. The two complexes [Mn(II)(terpy)Cl_2] and [Mn(III)(terpy)Cl_3] differ by the oxidation and spin-state ($S(Mn^{II}) = 5/2$ and $S(Mn^{III}) = 2$) of the central Mn ion and more importantly by the number of ligands and their coordination geometry. [Mn(III)(terpy)Cl_3] is six-coordinate whereas [Mn(II)(terpy)Cl_2] is a five-coordinate

dx.doi.org/10.1021/ic202229b | Inorg. Chem. 2012, 51, 680−687

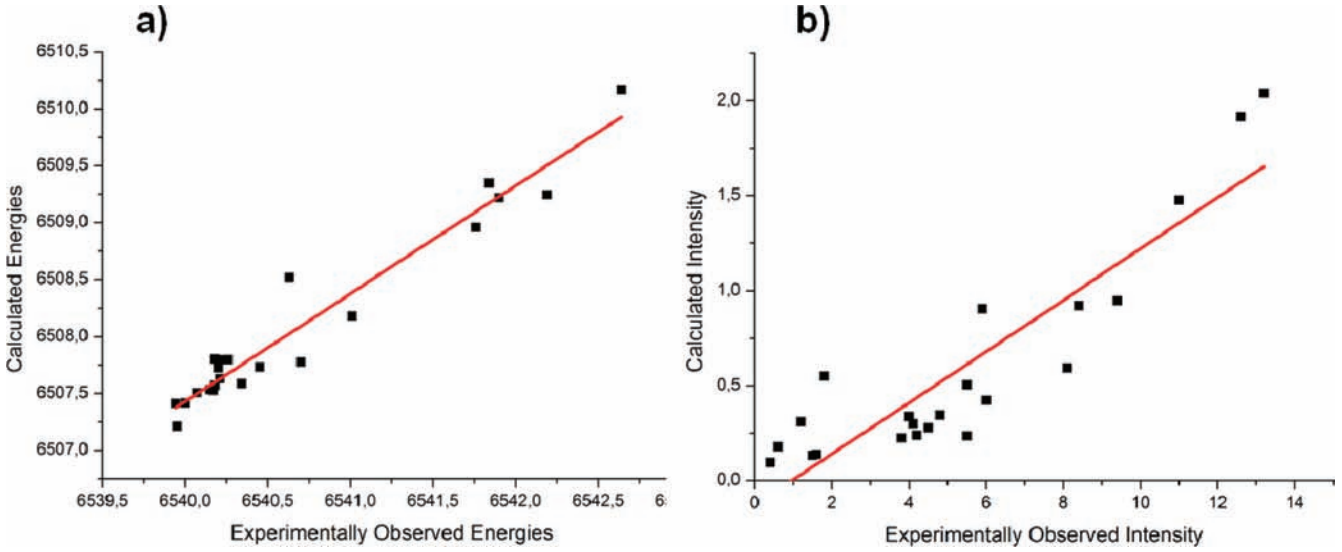

Figure 1. Relationship of calculated to experimentally determined transition energies (a) and intensities (b). The calculations used the B3LYP functional. The linear least-squares fits are given by: $f^{(a)} = 0.948E(\text{exp}) + 318.62$ eV and $f^{(b)} = 0.135I$ (exp) − 0.129.

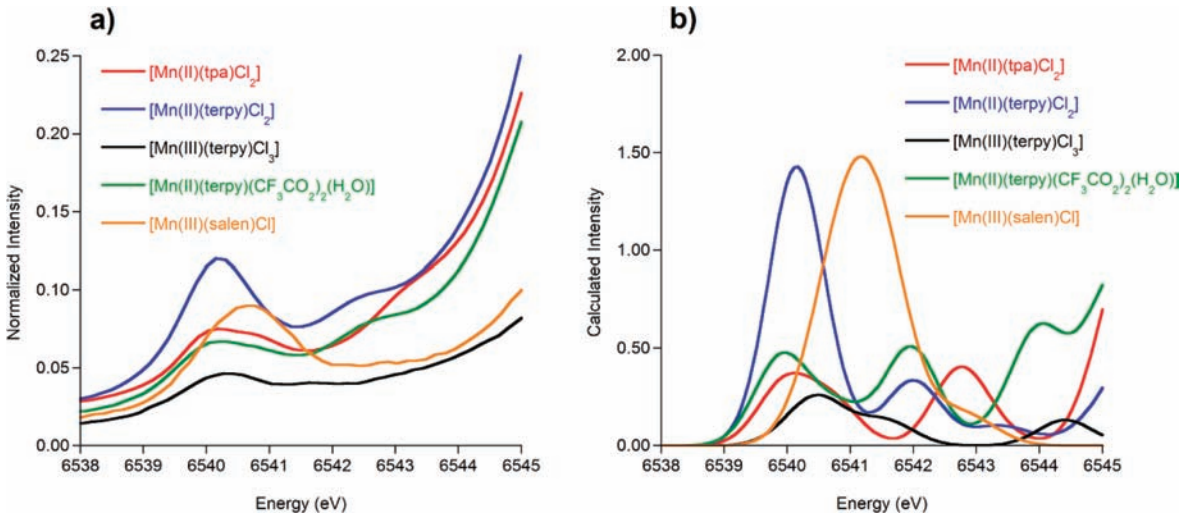

Figure 2. Experimental (a) and calculated (b) K pre-edge regions of various Mn-complexes highlighting the influence of geometrical parameters such as coordination number and geometry on the pre-edge intensity. The calculations used the B3LYP functional, and a 32.6 eV energy shift and 1 eV broadening have been applied to all calculated spectra.

complex. The six ligating atoms (3 × N and 3 × Cl) of $[Mn(III)(terpy)Cl_3]$ together form a slightly distorted octahedral environment around the central Mn^{3+} ion. The coordination sphere of the distorted square planar $[Mn(II)(terpy)Cl_2]$ complex, on the other hand, is arranged such that the two chloro ligands are above and below the plane that is described by the terpy ligand with a Cl−Mn−Cl angle of 114.9 degrees.

The pre-edges of both $[Mn(III)(terpy)Cl_3]$ and $[Mn(II)(terpy)Cl_2]$ each exhibit two features, one at 6540.2 eV and the other one to higher energy (~6542.3 eV). According to the calculations, the former is assigned as a standard Mn 1s to Mn 3d pre-edge transition, which gains some intensity because of 4p mixing. The second peak corresponds to a metal-to-ligand charge-transfer (MLCT) transition that will be discussed in detail in the next section.

The 1s to 3d transition of $[Mn(II)(terpy)Cl_2]$ is ~2.5 times more intense than for $[Mn(III)(terpy)Cl_3]$ in the experimental spectra. In the calculated spectra, the difference is even more pronounced with an intensity ratio of 3.3 to 1 (Figure 2 and Table 1). This significant increase in pre-edge intensity for $[Mn(II)(terpy)Cl_2]$ is readily attributed to the change in the coordination geometry. The 4p mixing into the Mn 3d-shell is more pronounced in square pyramidal geometry than in octahedral geometry, so the pre-edge transitions acquire more allowed electric dipole character in square pyramidal geometry.[49,12,2]

Similar observations can be made for the pre-edge of the six-coordinate $[Mn(II)(tpa)Cl_2]$ complex, which has the same oxidation and spin state as the five-coordinate $[Mn(II)(terpy)Cl_2]$ complex. It also has two pre-edge features, one corresponding to Mn 1s to 3d transitions (6540.2 eV) and the other due to MLCT processes (6543.2 eV). Because of the distorted octahedral coordination geometry, the low energy pre-edge feature has a low intensity compared to the 5-fold coordinated $[Mn(II)(terpy)Cl_2]$. Analogously, the quadratic

dx.doi.org/10.1021/ic202229b | Inorg. Chem. 2012, 51, 680−687

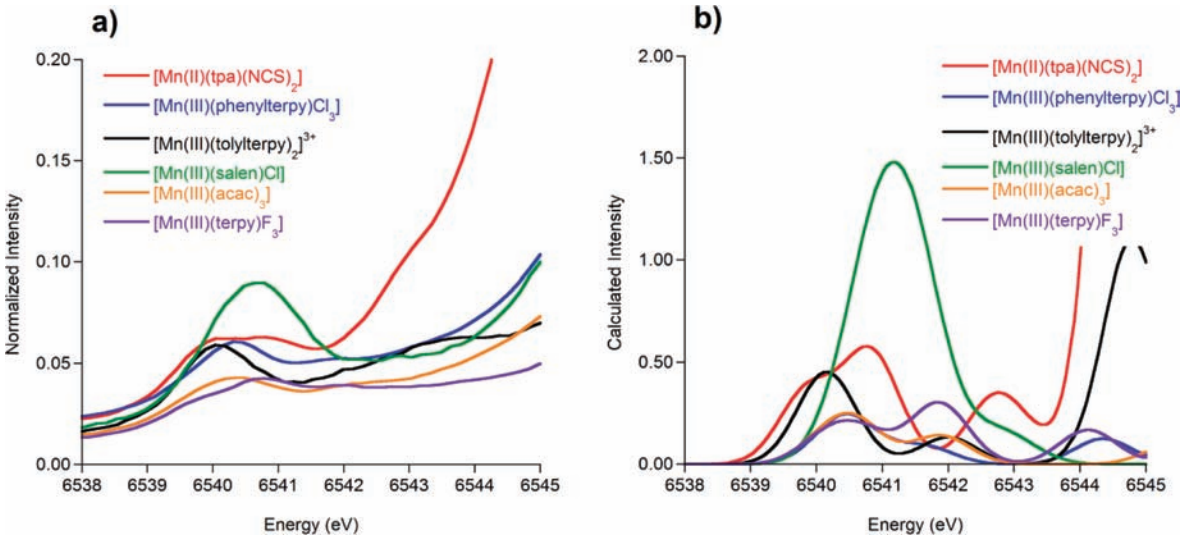

Figure 3. Experimental (a) and calculated (b) K pre-edge regions of various Mn-complexes highlighting their relatively strong ligand field. The calculations used the B3LYP functional, and a 32.6 eV energy shift and 1 eV broadening have been applied to all calculated spectra.

pyramidal coordination geometry of [Mn(III)(salen)Cl] leads to an enhanced pre-edge intensity. Thus, the present test set nicely confirms the generally accepted notion that six-coordinate complexes give rise to less intense pre-edge features than their five-coordinate counterparts.[1,2,11]

All measured and calculated spectra exhibit two or more features in the pre-edge region. The TD-DFT methodology readily allows for the assignment of the observed transitions. For most of the investigated compounds, the 1s to 3d transitions all contribute to a single pre-edge feature with one resolved maximum. This is because the "ligand field splitting" between the different final states arising from the $1s^1 3d^{N+1}$ configuration is smaller than the experimental resolution of around 1 eV (Figure 2). Only compounds with strong ligand fields exhibit two or more 1s to 3d features. In the present series of compounds only $[Mn(III)(acac)_3]$, $[Mn(III)(terpy)F_3]$, [Mn(III)(salen)Cl], $[Mn(III)(phenylterpy)Cl_3]$, $[Mn(III)(tolylterpy)_2]^{3+}$, and $[Mn(II)(tpa)(NCS)_2]$ show two resolved 1s to 3d bands in their pre-edge spectra (Figure 3). Most of these complexes contain a Mn^{3+} ion, which is consistent with the generally larger ligand field strength in Mn^{3+} complexes as compared to Mn^{2+} complexes. For example, the experimental spectrum of $[Mn(III)(acac)_3]$ shows two features with their maxima at 6540.2 and 6542.2 eV, corresponding to transitions into the t_{2g} and e_g derived molecular orbitals. This corresponds to a ligand field splitting of 2.0 eV. As is well-known, the spin-polarized picture does not properly resolve all of the final state multiplets.[50,51] In terms of the spin-polarized description, however, the excited state corresponding to the alpha 1s to t_{2g} transition is lowest in energy, thus contributing to the first experimentally observed feature. This can be explained by the strong spin polarization apparent in d^4 high-spin complexes. The same qualitative order of states was found for all complexes exhibiting two 1s to 3d features. For $[Mn(III)(acac)_3]$ the employed TD-DFT method underestimates the splitting of the 1s to 3d features by 0.5 eV (calculated at 6540.4 and 6541.9 eV, vs 6540.2 and 6542.2 eV from experiment, Table 1). Similar observations are made for $[Mn(III)(phenylterpy)Cl_3]$, $[Mn(III)(tolylterpy)_2]^{3+}$, and [Mn(III)(salen)Cl] where TD-DFT underestimates the splitting by 0.3, 0.4, and 0.8 eV, respectively (Table 1). The ligand field splitting for $[Mn(II)(tpa)(NCS)_2]$ is much better reproduced by TD-DFT with experimental and calculated values of 1.0 and 0.9 eV, respectively. The experimental spectrum of $[Mn(III)(terpy)F_3]$ exhibits three distinguishable 1s to 3d features. This remarkable observation is due to relatively short Mn−F bond distances (with optimized bond distances of 1.83 Å), which in turn lead to a strong ligand field. Again, TD-DFT underestimates the ligand field splitting resulting, in this particular case, in a qualitatively incorrect spectrum with only two resolved 1s to 3d features. Nevertheless, the theoretical results for the well-localized transitions into the predominantly empty metal 3d-orbitals are reasonable to good. Problems, however, are apparent with charge transfer transitions, as discussed below.

Ligands with Extended π-Systems. The experimental and calculated XAS pre-edge region of $[Mn(II)(terpy)Cl_2]$ is shown in Figure 4a and b. This molecule will serve as an example to gain insight into the nature of the predicted spectra for the class of compounds containing ligands that have extended, arylic π-systems. Similar results are obtained for complexes that contain the acac, tpa, phenylterpy, tolylterpy, or tBu_3terpy ligands. These ligands are primarily of π-donor character but nevertheless have low-lying empty π^* orbitals.

To emphasize certain aspects of the TD-DFT method, we chose to present a spectrum that was calculated with a non-hybrid density functional (BP86). Both experimental and calculated spectra exhibit two features that are separated by 2 eV. In the experimental spectrum, the more intense peak is situated at lower energy, whereas in the calculated spectrum the relative intensities of the two resolved peaks are reversed. This erroneous behavior is due to the well-known fact that TD-DFT has severe problems with excited states of charge transfer character. Depending on the system and the amount of exact exchange in the functional, such transitions can appear several eV too low in the calculated spectra. This is well-known from valence excited states in the UV and visible regions of the spectrum,[52,53] but appears to also hold for XAS calculations. The same behavior is met here, where the extended π-systems of the ligands give rise to charge transfer artifacts or what we will also term as "ghost-states". The effect of increasing the amount of HF exchange on the predicted pre-edge spectrum of $[Mn(II)(terpy)Cl_2]$ is demonstrated in Figure 5 where the

dx.doi.org/10.1021/ic202229b | Inorg. Chem. 2012, 51, 680−687

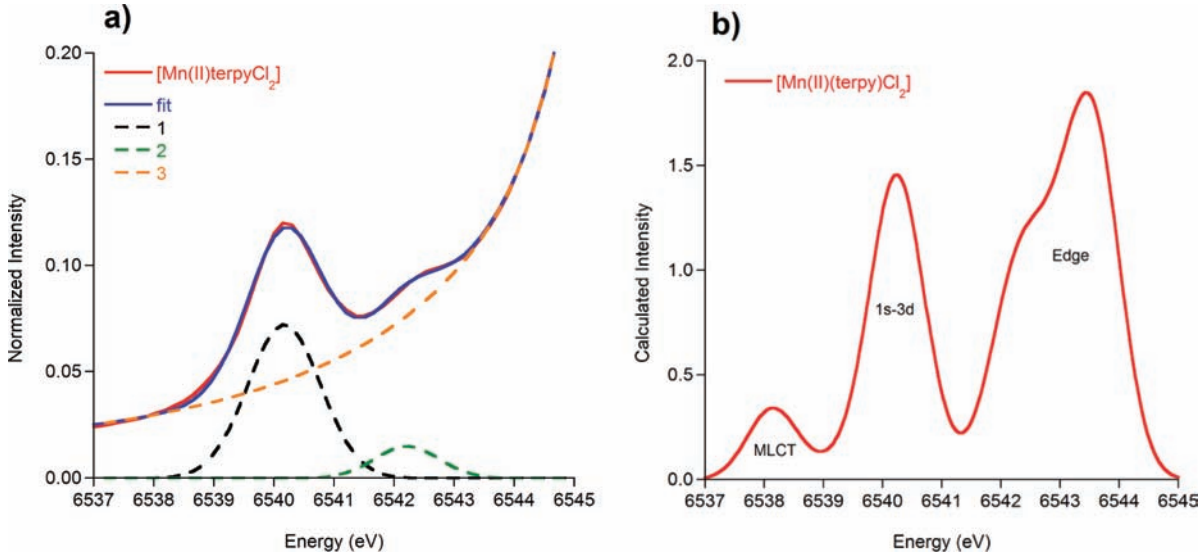

Figure 4. Experimental (a) and calculated (b) pre-edge spectra of $[Mn(II)(terpy)Cl_2]$. The dashed lines in the experimental spectrum represent the individual pre-edge (green and black dashed lines) and background component (orange dashed line) of the fit. The fit to the pre-edge comprises two features, one intense metal 1s to 3d peak at lowest energy (black dashed line) and a weak MLCT peak to higher energy (green dashed line). The calculation used the BP86 functional and hence the MLCT absorption occurs at lower energies. A 62.3 eV energy shift and 1 eV broadening have been applied to the calculated spectrum.

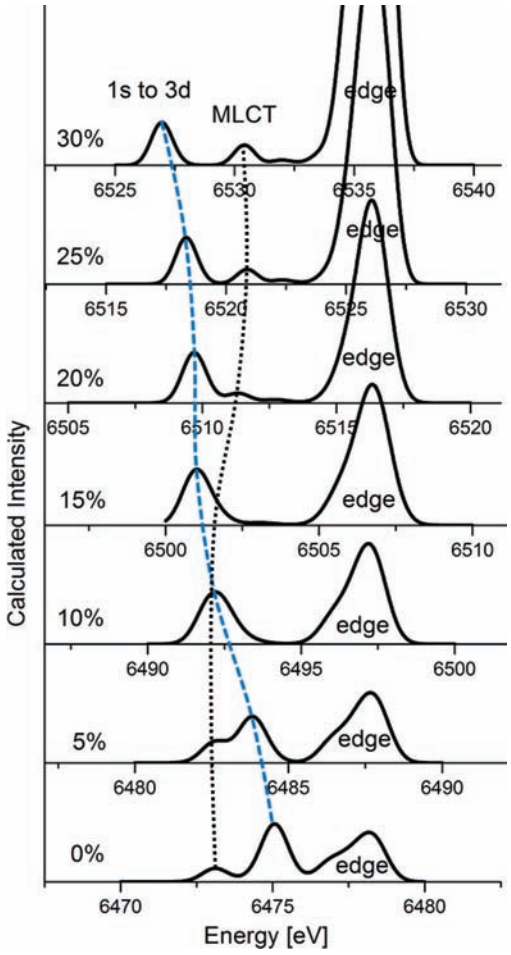

Figure 5. Calculated spectra of $[Mn(II)(terpy)Cl_2]$ with a series of functionals with a varying amount of HF exchange. Starting with no HF exchange, the percentage increases in steps of 5% up to a maximum of 30% HF exchange. It is seen that the position of the MLCT peak (black dotted line) relative to the 1s to 3d peak (blue dashed line) changes from lower in energy (0%, 5%) to the same energy (10%, 15%) to higher energy (20% and higher) depending on the amount of HF exchange.

fraction of HF exchange varies from 0% to 30%. The most obvious effect is that the absolute transition energies increase with increasing amount of HF exchange. Second, the rising edge feature becomes more pronounced, which is due to the fixed number of calculated roots (40). Since the number of calculated "ghost-states" is reduced as the amount of HF exchange is increased,[52] more states that belong to the edge feature of the spectrum are included in the calculation. Hence, the calculated edge feature gains intensity when more HF exchange is present. The most important effect for the present work, however, is that the MLCT feature in the calculated spectrum is, as expected, shifted relative to the 1s-3d absorption to higher energies. Moreover the intensity of the MLCT-feature is slightly reduced with increasing amount of HF exchange. A detailed analysis of this series and a similar study for $[Mn(II)(tolylterpy)_2]^{2+}$, which has a more pronounced MLCT feature, revealed that an admixture of 22% HF exchange yields the best results in terms of energy splitting and intensity ratio. This will be further addressed in the conclusion section.

Effect of π-Acceptor Ligands. Pre-edge spectra of compounds containing ligands with considerable π-acceptor character such as N_3^- or SCN^- exhibit remarkable features in the rising edge-region of the Mn K-edge XAS spectra. Figure 6 shows the experimental and calculated spectra of $[Mn(II)(tpa)Cl_2]$ and $[Mn(II)(tpa)(NCS)_2]$. The calculated spectrum of $[Mn(II)(tpa)(NCS)_2]$ shows a strong feature at high energy that appears as a shoulder on the rising edge in the experimental spectrum. In our calculations, these features can be reproduced even within a relatively small number of calculated excited states. A proper reproduction of the rising edge features is unfortunately not feasible with the restrictions imposed by standard basis sets and DFT potentials. According to the calculations, the excited states that correspond to this strong feature have dominantly MLCT character. However, they are one order of magnitude more intense than the "ghost" MLCT transitions described in the previous section of the paper. This finding can be rationalized by the nature of the acceptor orbitals that are associated with the excited states. The acceptor

dx.doi.org/10.1021/ic202229b | Inorg. Chem. 2012, 51, 680–687

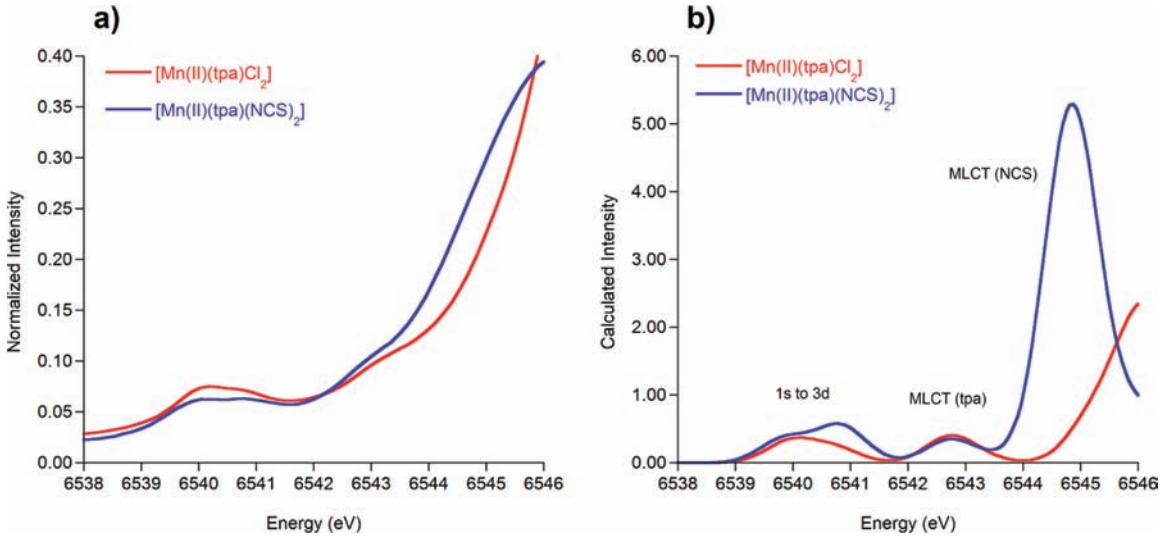

Figure 6. Experimental (a) and calculated (b) pre-edge spectra of $[Mn(II)(tpa)Cl_2]$ and $[Mn(II)(tpa)(NCS)_2]$. The calculations used the B3LYP functional, and a 32.64 eV energy shift and 1 eV broadening have been applied to the calculated spectra. Both spectra exhibit features corresponding to Mn 1s to 3d transitions around 6540.5 eV and a MLCT band at ~6542.8 eV. Only the spectrum of $[Mn(II)(tpa)(NCS)_2]$ has an additional, intense MLCT band at 6545 eV due to transitions into π-orbitals of the NCS^- ligand. The high energy feature at 6546 eV of $[Mn(II)(tpa)Cl_2]$ is] the onset of the rising edge.

orbitals associated with strong features have mostly SCN^- π-antibonding character. Strong metal-to-ligand backbonding interactions lead to mixing of metal d- and p- orbitals with the empty ligand orbitals. Hence, transitions from the metal 1s orbital to these orbitals gain intensity. Similar observations have been made for $[Mn(III)(bpea)(N_3)_3]$, $[Mn(III)(terpy)(N_3)_3]$, and $[Mn(II)(tbu_3terpy)(N_3)_2]$. Due to the MLCT character of the excited states that lead to the features discussed here, the predicted transition energies suffer from the same problems of the DFT method as described above. Nevertheless, we are not aware of any previous study that connects the π-acceptor character of the ligands to observable shoulders of the metal K-edge.

CONCLUSIONS

In this work, we have extended the previously reported method of calculating XAS K-edge pre-edge spectra with a simple TD-DFT protocol to Mn K-edges using different density functionals. We have found that as for iron, chlorine, and sulfur K-edges,[15−17] the shape, intensity, and position of Mn 1s to 3d transitions is well predicted by TD-DFT. However, we have shown that the prediction of MLCT transitions is more problematic and may lead to significant artifacts in the calculated spectra.[54] Our series of mononuclear coordination compounds contains many examples of ligands that interact with the central manganese ion via π-orbitals. Among this set one can discriminate between ligands with extended, arylic π-systems and genuine π-acceptor ligands such as the azide or thiocyanate ion. The former give rise to rather weak features 1−3 eV higher in energy than the main metal 1s to 3d peak. Although their exact position in the calculated spectrum is highly dependent on the amount of HF exchange incorporated in the functional and by no means predictive, their existence and appearance is qualitatively correct. It has to be noted that in the case of calculations with the TPSSh functional (Supporting Information), the MLCT transitions for some of these systems coincide with the metal 1s to 3d peak. This may lead to the wrong number of peaks in the calculated spectrum. Ligands of primarily π-acceptor character cause intense absorptions at high energies, which appear as clearly visible shoulders on the edge. These features are well reproduced by the TD-DFT method although their predicted position deviates in some cases from the measured values. Spectra calculated with 22% of exact exchange match the experimental spectra well. However, such agreement is, in our opinion, treacherous. It is well-known from the closely related problems of hyperfine structure or spin-state energetics calculations, that there is not a single fraction of HF exchange that is universally applicable to complexes containing different metals in different oxidation states.[55] In this respect, one should rather be aware of the shortcomings of the functionals used, which means that for XAS calculations one has to be careful when calculating spectra for complexes with extended π-ligand systems. As in many other instances, the 20% exact exchange used in the B3LYP functional appears to be a sensible compromise. In the longer run, of course, systematic improvements to TD-DFT are necessary. In particular, there is growing evidence that range-corrected density functionals represent a significant improvement.[56−58] Furthermore, orbital relaxation should be incorporated into TD-DFT. Work along these lines is in progress in our research groups.

The present work lays the foundation of the application of the TD-DFT methodology to highly important problems in manganese biochemistry, foremost of course the tetranuclear manganese cluster in PSII. However, before this problem can be successfully addressed it must be proven that the methodology is applicable to spin-coupled oligonuclear systems. Work along these lines will be reported in due course.

ASSOCIATED CONTENT

Supporting Information

Complete comparison of experimental and calculated pre-edge spectra for B3LYP. Pre-edge spectrum of $[Mn(II)(terpy)Cl_2]$ calculated with TPSSh. Linear fit data for transition energies and intensities for TPSSh, BP, and BLYP(22%). This material is available free of charge via the Internet at http://pubs.acs.org.

dx.doi.org/10.1021/ic202229b | Inorg. Chem. 2012, 51, 680−687

AUTHOR INFORMATION

Corresponding Author

*E-mail: frank.neese@mpi-mail.mpg.de (F.N.), serena.debeer@mpi-mail.mpg.de (S.D.).

ACKNOWLEDGMENTS

Cornell University (S.D.), the University of Bonn (F.N.), the Alfred P. Sloan Foundation (S.D.), and the Max-Planck Society (S.D. and F.N.) are gratefully acknowledged for support. Portions of this research were carried out at the Stanford Synchrotron Radiation Lightsource, a national user facility operated by Stanford University on behalf of the DOE, BES. The SSRL SMB Program is supported by DOE, BER, and NIH, NCRR, BMTP.

REFERENCES

(1) Roe, A. L.; Schneider, D. J.; Mayer, R. J.; Pyrz, J. W.; Widom, J.; Que, L. Jr. *J. Am. Chem. Soc.* **1984**, *106*, 1676.
(2) Westre, T. E.; Kennepohl, P.; DeWitt, J. G.; Hedman, B.; Hodgson, K. O.; Solomon, E. I. *J. Am. Chem. Soc.* **1997**, *119*, 6297.
(3) Grunes, L. *Phys. Rev. B* **1983**, *27*, 2111.
(4) Dau, H.; Iuzzolino, L.; Dittmer, J. *Biochim. Biophys. Acta, Bioenerg.* **2001**, *1503*, 24.
(5) Berry, J. F.; Bill, E.; Bothe, E.; DeBeer George, S.; Mienert, B.; Neese, F.; Wieghardt, K. *Science* **2006**, *312*, 1937.
(6) Berry, J. F.; DeBeer George, S.; Neese, F. *Phys. Chem. Chem. Phys.* **2008**, *10*, 4361.
(7) Song, W. J.; Seo, M. S.; DeBeer George, S.; Ohta, T.; Song, R.; Kang, M.-J.; Tosha, T.; Kitagawa, T.; Solomon, E. I.; Nam, W. *J. Am. Chem. Soc.* **2007**, *129*, 1268.
(8) Shadle, S. E.; Penner-Hahn, J. E.; Schugar, H. J.; Hedman, B.; Hodgson, K. O.; Solomon, E. I. *J. Am. Chem. Soc.* **1993**, *115*, 767.
(9) Aliaga-Alcalde, M.; DeBeer George, S.; Mienert, B.; Bill, E.; Wieghardt, K.; Neese, F. *Angew. Chem., Int. Ed.* **2005**, *44*, 2908.
(10) Jaszewski, A. R.; Stranger, R.; Pace, R. J. *J. Phys. Chem. A* **2008**, *112*, 11223.
(11) Randall, C. R.; Shu, L.; Chiou, Y.-M.; Hagen, K. S.; Ito, M.; Kitajima, N.; Lachicotte, R. J.; Zang, Y.; Que, L. *Inorg. Chem.* **1995**, *34*, 1036.
(12) Shulman, G.; Yafet, Y.; Eisenberger, P.; Blumberg, W. *Proc. Natl. Acad. Sci. U. S. A.* **1976**, *73*, 1384.
(13) Hahn, J. E.; Scott, R. A.; Hodgson, K. O.; Doniach, S.; Desjardins, S. R.; Solomon, E. I. *Chem. Phys. Lett.* **1982**, *88*, 595.
(14) Dräger, G.; Frahm, R.; Materlik, G.; Brümmer, O. *Phys. Status Solidi B* **1988**, *146*, 287.
(15) DeBeer George, S.; Petrenko, T.; Neese, F. *J. Phys. Chem. A* **2008**, *112*, 12936.
(16) DeBeer George, S.; Petrenko, T.; Neese, F. *Inorg. Chim. Acta* **2008**, *361*, 965.
(17) DeBeer George, S.; Neese, F. *Inorg. Chem.* **2010**, *49*, 1849.
(18) Beckwith, M. A.; Roemelt, M.; Collomb, M. N.; DuBoc, C.; Weng, T.-C.; Bergmann, U.; Glatzel, P.; Neese, F.; DeBeer, S. *Inorg. Chem.* **2011**, *50*, 8397.
(19) Yano, J.; Kern, J.; Sauer, K.; Latimer, M. J.; Pushkar, Y.; Biesiadka, J.; Loll, B.; Saenger, W.; Messinger, J.; Zouni, A.; Yachandra, V. K. *Science* **2006**, *314*, 821.
(20) Yano, J.; Yachandra, V. K. *Inorg. Chem.* **2008**, *47*, 1711.
(21) Mantel, C.; Hassan, A. K.; Pécaut, J.; Deronzier, A.; Collomb, M. N.; Duboc-Toia, C. *J. Am. Chem. Soc.* **2003**, *125*, 12337.
(22) Mantel, C.; Chen, H. Y.; Crabtree, R. H.; Brudvig, G. W.; Pécaut, J.; Collomb, M. N.; Duboc, C. *ChemPhysChem* **2005**, *6*, 541.
(23) Limburg, J.; Vrettos, J. S.; Crabtree, R. H.; Brudvig, G. W.; Paula, J. C. d.; Hassan, A.; Barra, A.-L.; Duboc-Toia, C.; Collomb, M.-N. *Inorg. Chem.* **2001**, *40*, 1698.
(24) Romain, S.; Duboc, C.; Neese, F.; Rivière, E.; Hanton, L. R.; Blackman, A. G.; Philouze, C.; Leprêtre, J.-C.; Deronzier, A.; Collomb, M.-N. *Chem.—Eur. J.* **2009**, *15*, 980.
(25) Duboc, C.; Collomb, M. N.; Pécaut, J.; Deronzier, A.; Neese, F. *Chem.—Eur. J.* **2008**, *14*, 6498.
(26) Mantel, C.; Philouze, C.; Collomb, M. N.; Duboc, C. *Eur. J. Inorg. Chem.* **2004**, 3880.
(27) Mantel, C.; Baffert, C.; Romero, I.; Deronzier, A.; Pécaut, J.; Collomb, M. N.; Duboc, C. *Inorg. Chem.* **2004**, *43*, 6455.
(28) Baffert, C.; Romero, I.; Pécaut, J.; Llobet, A.; Deronzier, A.; Collomb, M.-N. *Inorg. Chim. Acta* **2004**, *357*, 3430.
(29) Rich, J.; Castillo, C. E.; Romero, I.; Rodríguez, M.; Duboc, C.; Collomb, M. N. *Eur. J. Inorg. Chem.* **2010**, 3658.
(30) Romain, S.; Baffert, C.; Duboc, C.; Lepretre, J. C.; Deronzier, A.; Collomb, M. N. *Inorg. Chem.* **2009**, *48*, 3125.
(31) Duboc, C.; Phoeung, T.; Zein, S.; Pécaut, J.; Collomb, M.-N.; Neese, F. *Inorg. Chem.* **2007**, *46*, 4905.
(32) Ray, K.; DeBeer George, S.; Solomon, E. I.; Wieghardt, K.; Neese, F. *Chem.—Eur. J* **2007**, *13*, 2783.
(33) Neese, F. *ORCA-an ab initio,density functional and semiempirical program package*, Version 2.7; University of Bonn: Bonn, Germany, 2010.
(34) Lenthe, E. v.; Baerends, E. J.; Snijders, J. G. *J. Chem. Phys.* **1993**, *99*, 4597.
(35) van Wüllen, C. *J. Chem. Phys.* **1998**, *109*, 392.
(36) Becke, A. D. *Am. Phys. Soc.* **1988**, *38*, 3098.
(37) Perdew, J. P. *Phys. Rev. B* **1986**, *33*, 8822.
(38) Pantazis, D. A.; Chen, X. Y.; Landis, C. R.; Neese, F. *J. Chem. Theory. Comput.* **2008**, *4*, 908.
(39) Weigend, F.; Ahlrichs, R. *Phys. Chem. Chem. Phys.* **2005**, *7*, 3297.
(40) Weigend, F. *Phys. Chem. Chem. Phys.* **2006**, *8*, 1057.
(41) Klamt, A.; Schüürmann, G. *J. Chem. Soc., Perkin Trans. 2* **1993**, 799.
(42) Hirata, S.; Head-Gordon, M. *Chem. Phys. Lett.* **1999**, *314*, 291.
(43) Becke, A. D. *J. Chem. Phys.* **1993**, *98*, 5648.
(44) Lee, C. T.; Yang, W. T.; Parr, R. G. *Phys. Rev. B* **1988**, *37*, 785.
(45) Staroverov, V. N.; Scuseria, G. E.; Tao, J.; Perdew, J. P. *J. Chem. Phys.* **2003**, *119*, 12129.
(46) Stephens, P. J.; Devlin, F. J.; Chabalowski, C. F.; Frisch, M. J. *J. Phys. Chem.* **1994**, *98*, 11623.
(47) Vosko, S. H.; Wilk, L.; Nusair, M. *Can. J. Phys.* **1980**, *58*, 1200.
(48) Neese, F.; Wennmohs, F.; Hansen, A.; Becker, U. *Chem. Phys.* **2009**, *356*, 98.
(49) Griffith, J. S. *The Theory of Transition Metal Ions*; Cambridge University Press: Cambridge, U.K., 1964.
(50) Neese, F.; Petrenko, T.; Ganyushin, D.; Olbrich, G. *Coord. Chem. Rev.* **2007**, *251*, 288.
(51) Tchougréeff, A. L.; Ángyán, J. G. *Int. J. Quantum Chem.* **2010**, *110*, 454.
(52) Neese, F. *J. Biol. Inorg. Chem.* **2006**, *11*, 702.
(53) Tozer, D. J. *J. Chem. Phys.* **2003**, *119*, 12697.
(54) Görling, A. *Chem. Phys. Lett.* **2006**, *419*, 517.
(55) Neese, F. *Coord. Chem. Rev.* **2009**, *253*, 526.
(56) Vydrov, A.; Heyd, J.; Krukau, A. V.; Scuseria, G. E. *J. Chem. Phys.* **2006**, *125*, 074106.
(57) Dreuw, A.; Weisman, J. L.; Head-Gordon, M. J. *Chem. Phys.* **2003**, *119*, 2943.
(58) Tawada, Y.; Tsuneda, T.; Yanagisawa, S.; Yanai, T.; Hirao, K. *J. Chem. Phys.* **2004**, *120*, 8425.